Supporting Information

Decoupled Tin−Silver Batteries with Long Cycle Life and Power Output Stability Based on Dendrite-Free Tin Anode and Halide Insertion Cathode Chemistry

Feifei Shi, Yudong Wu, Binyan Wang, Jiawei Bai, Yihan Ren, Tao Yang, Funian Mo, Derek Ho, and Haibo Hu**

F. F. Shi, Dr. Y. D. Wu and Prof. H. B. Hu
School of Materials Science and Engineering, Anhui University, Hefei 230601, China.
Email: haibohu@ahu.edu.cn

B. Y. Wang, J. W. Bai, Y. H. Ren and Prof. H. B. Hu
Stony Brook Institute at Anhui University, Anhui University, Hefei 230039, China.

Prof. T. Yang
Centre for Mechanical Technology and Automation, Department of Mechanical Engineering, University of Aveiro, Aveiro 3810-193, Portugal.

Dr. F. N. Mo
School of Future Technology, Shenzhen Technology University, Shenzhen 518055, China.
Email: mofunian@sztu.edu.cn

Prof. D. Ho
Department of Materials Science and Engineering, City University of Hong Kong, Kowloon, Hong Kong 999077, China

Prof. D. Ho
Hong Kong Center for Cerebro-Cardiovascular Health Engineering, Hong Kong 999077, China

Keywords: decoupled Sn–Ag cell, Sn anodes, dendrite-free, cyclic stability, Ag nanowires

Experimental section

Synthesis of Ag nanowires:

Ag nanowires (AgNWs) were prepared by a polyol process. Firstly, 0.72 g of polyvinylpyrrolidone (PVP) was dissolved into 100 mL ethylene glycol (EG) in an oil bath at 130 °C. Then, $AgNO_3$ (800 mg) and $FeCl_3$ (15 mg) were added into the above solution. Subsequently, the mixed solution was heated up to 160 °C without stirring for 50 mins. After further cooling the solution to room temperature, the AgNWs were obtained by filtering the mixture and washing with DI water. Finally, 120 mg of purified AgNWs were dispersed in 48 mL DI water containing PVP to obtain an AgNWs colloid solution for further use (2.5 mg/mL).

Preparation of AgNWs/CNTs hybrid film:

Firstly, 40 mL commercialized carbon nanotube (CNTs) solution (2.5 mg/mL) was added to 40 mL AgNWs colloid solution (2.5 mg/mL) under stirring to prepare a mixed solution. Then, the AgNWs/CNTs hybrid film was obtained via filtering the above mixed solution, which was further peeled off from the filter membrane and dried for 24 h.

Assembly of the decoupled Sn–Ag and Zn–Ag cells:

The designed Sn–Ag cell comprises two chambers separated by a cation-exchange membrane (TCEM8040, HangZhou Huamo Technology Co., Ltd.), each containing different electrolytes. Specifically, other components utilized include Sn foil (anode), an alkaline solution (1 M $K_2Sn(OH)_6$/0.5 M KOH, anolyte), a neutral solution (2.5 M KCl, catholyte), AgNWs/CNTs hybrid film (cathode), and a titanium plate (current collector). The scheme of the cell structure is shown in **Figure S15** of the Supporting Information. The effective area of both Sn foil and the AgNWs/CNTs hybrid film are 0.5 cm^2. Subsequently, 0.2 ml of anolyte and 0.2 mL of a catholyte were added to the alkaline chamber and neutral chamber respectively. Finally, the decoupled Sn–Ag cell was tested at room temperature after 2 hours of standing. For comparison, a decoupled Zn–Ag cell was fabricated following the same steps. The Zn–Ag cell comprises a Zn anode in an alkaline electrolyte (0.5 M KOH/0.025 M ZnO) and the same AgNWs/CNTs hybrid cathode in a neutral electrolyte (0.5 M KCl).

Assembly and demonstration of the intelligent power system:

Based on the designed power management circuits (**Figure 6f**), two commercial solar cells (output voltage 2 V/sunlight) are connected in series with decoupled Sn-Ag battery (stable output voltage 1.1 V) form to establish a solar-to-energy integrated system. Subsequently, the solar-to-energy integrated system is connected with an LED

(operating voltage of 1 V) to demonstrate its actual application scenarios.

The power management circuit automatically controls the lighting and extinguishing of the LED by detecting the voltage of the solar cells. When the energy converted by the solar cells reaches the voltage threshold of 2 V, the controller considers it as daytime and automatically adjusts the program accordingly. It connects the decoupled Sn-Ag battery to the solar cell for charging and disconnects the connection between the battery and the LED, preventing the LED from turning on. When the energy converted by the solar cells does not reach the set voltage, the controller determines it is nighttime. At this point, the controller automatically adjusts the program by disconnecting the decoupled Sn-Ag battery from the solar cells and connecting the LED to the battery, thus activating the illumination. This achieves the purpose of charging during the day and automatically lighting up at night.

Electrochemical measurements:

Long-term depositing/stripping performance of Sn||Sn symmetric cell utilizing an alkaline (1 M $K_2Sn(OH)_6$/0.5 M KOH) and Zn||Zn symmetric cells respectively employing neutral (1.25 M $ZnCl_2$) and alkaline (0.5 M KOH/0.025 M ZnO) electrolytes were tested by LAND multi-channel battery test system (CT2001A, China). Cyclic voltammetry (CV), galvanostatic charge–discharge (GCD), and electrochemical impedance spectroscopy (EIS) (in the frequency range between 100 kHz and 0.01 Hz with an amplitude of ±10 mV at an open-circuit potential) measurements of the decoupled cells were conducted using an electrochemical workstation (CHI 760E, Chenhua). Cycling measurement was carried out on a LAND multi-channel battery test system (CT2001A, China) at room temperature.

Material Characterizations:

The microstructure and phase composition of the samples were revealed by Field-emission scanning electron microscopy (FE-SEM, S-4800, Hitachi, Japan), Transmission electron microscopy (TEM, JEM-2100, JEOL, Japan), and X-ray powder diffraction (XRD Bruker D8-ADVANCE) with an 18 kW advanced X-ray diffrac-tometer with Cu Kα radiation (λ=1.54056Å). 3D optical images (500x magnification) were obtained by an ultra-depth three-dimensional microscope (Keyence, VH-Z500R).

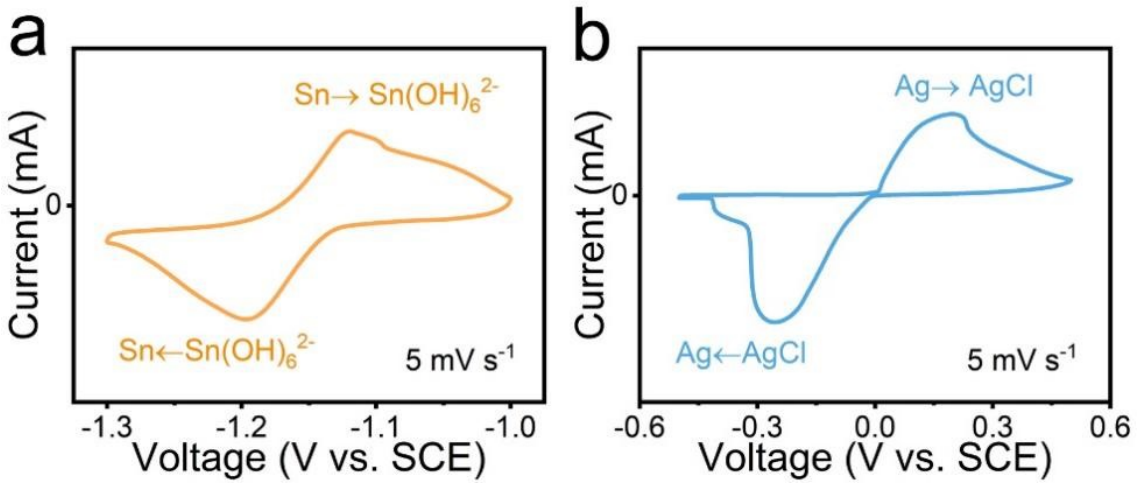

Figure S1. CV curves of (a) the Sn anode in 1 M $K_2Sn(OH)_6$+0.5 M KOH and b) the AgNWs/CNTs cathode in 2.5 KCl. (Sn foil and the AgNWs/CNTs cathode as working electrode respectively, a graphite rod as the counter electrode, and a saturated calomel reference electrode (SCE) as the reference electrode).

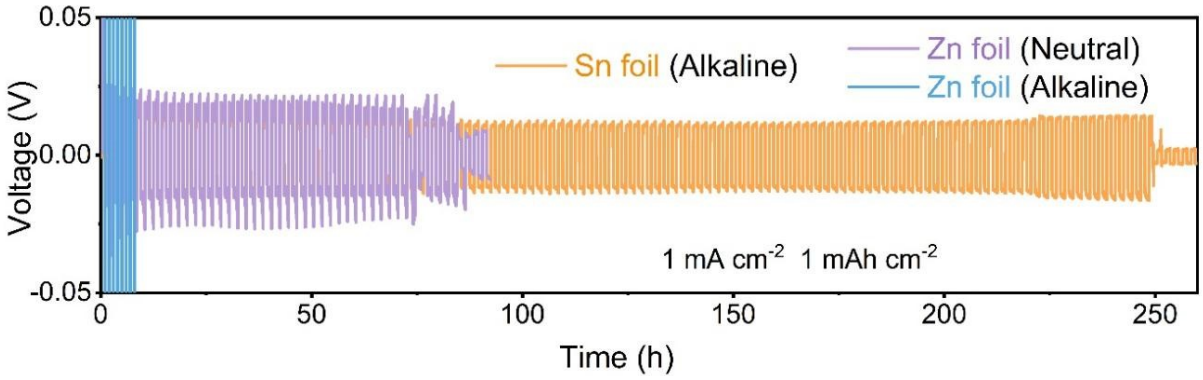

Figure S2. Comparison of cyclic performance between Sn||Sn and Zn||Zn symmetric coin-type cells with neutral and alkaline electrolytes, respectively. (The Zn||Zn symmetric cell in an alkaline electrolyte fails at the first several cycle, the Zn||Zn symmetric cell with neutral electrolyte is unstable after 70 cycles, the Sn||Sn symmetric cell in the alkaline electrolyte fails after 220 cycles).

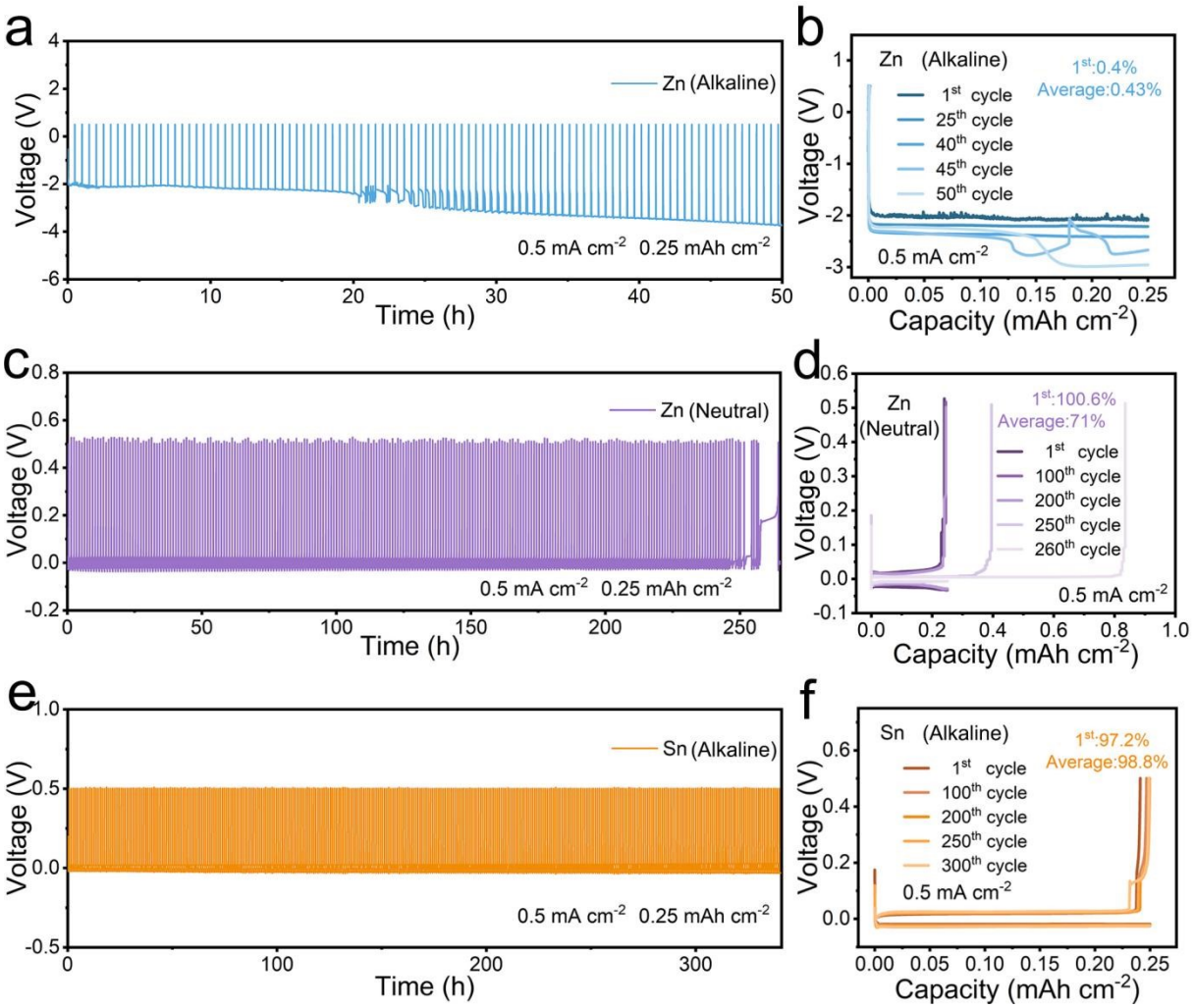

Figure S3. a, c, e) Galvanostatic electrodeposition/dissolution profiles of the Zn||Cu and Sn||Cu asymmetrical half-cells with different electrolytes at the current density of 0.5 mA cm^{-2} and cutoff capacity of 0.25 mAh cm^{-2}. b, d, f) The corresponding detailed charge-discharge profiles.

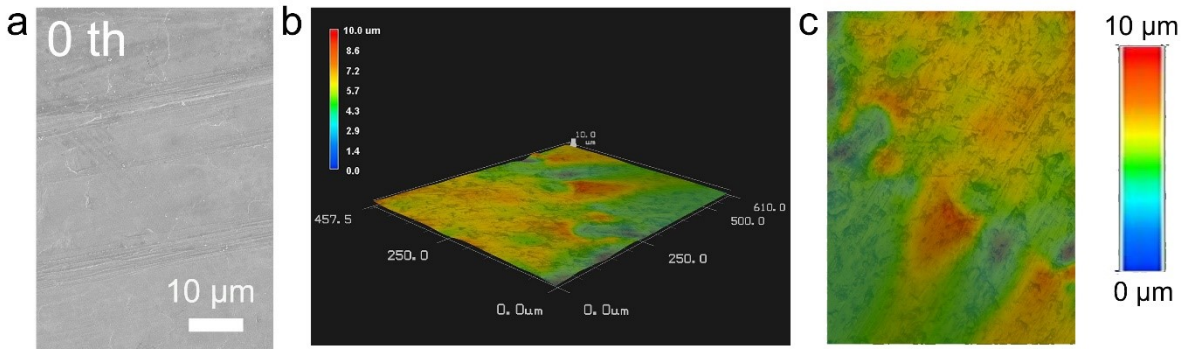

Figure S4. a) SEM image of pristine Zn after 0th cycle. The corresponding optical surface profilometry image of b) 3D and c) 2D features.

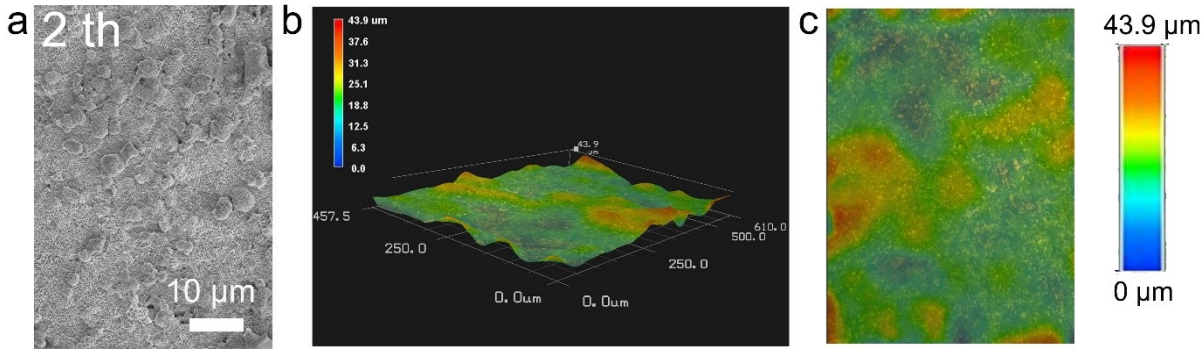

Figure S5. a) SEM image of Zn electrode after 2th cycle in alkaline electrolyte. The corresponding optical surface profilometry image of b) 3D and c) 2D features.

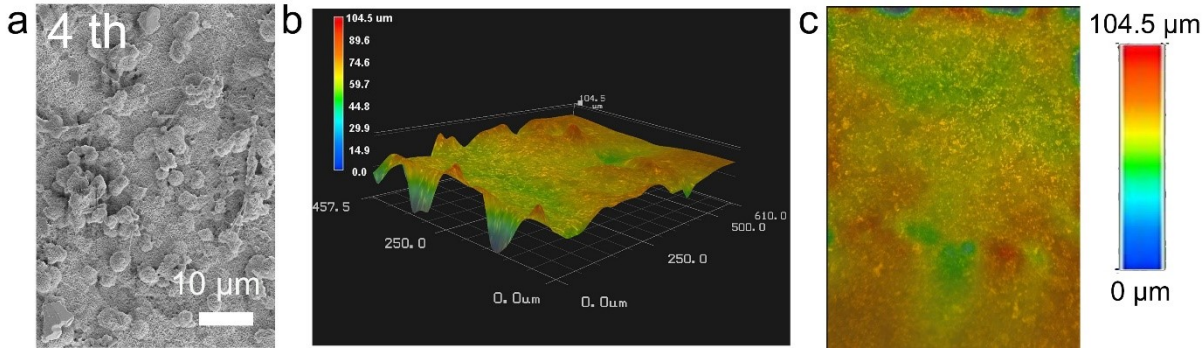

Figure S6. a) SEM image of Zn electrode after 6th cycle in alkaline electrolyte. The corresponding optical surface profilometry image of b) 3D and c) 2D features.

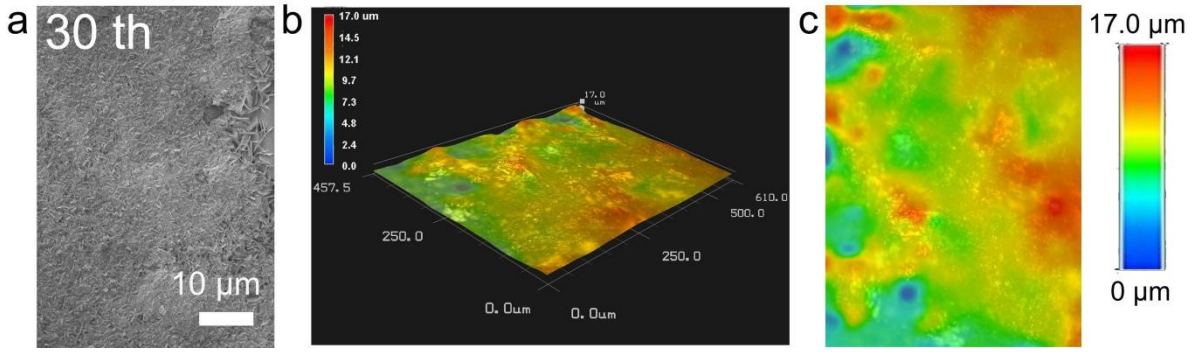

Figure S7. a) SEM image of pristine Zn after 30th cycle in neutral electrolyte. The corresponding optical surface profilometry image of b) 3D and c) 2D features.

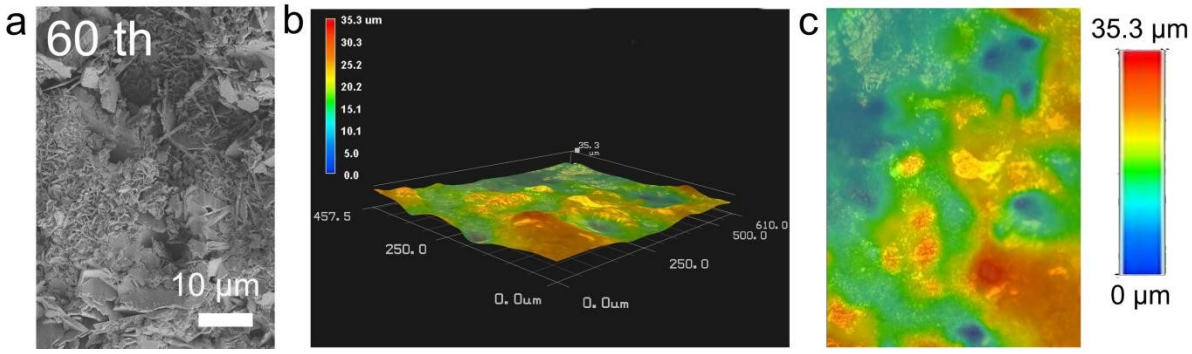

Figure S8. a) SEM image of pristine Zn after 60th cycle in neutral electrolyte. The corresponding optical surface profilometry image of b) 3D and c) 2D features.

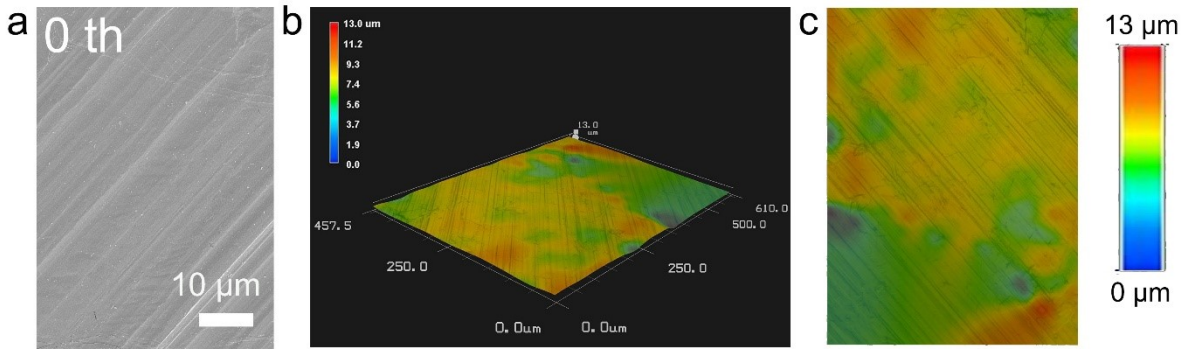

Figure S9. a) SEM image of pristine Sn after 0th cycle. The corresponding optical surface profilometry image of b) 3D and c) 2D features.

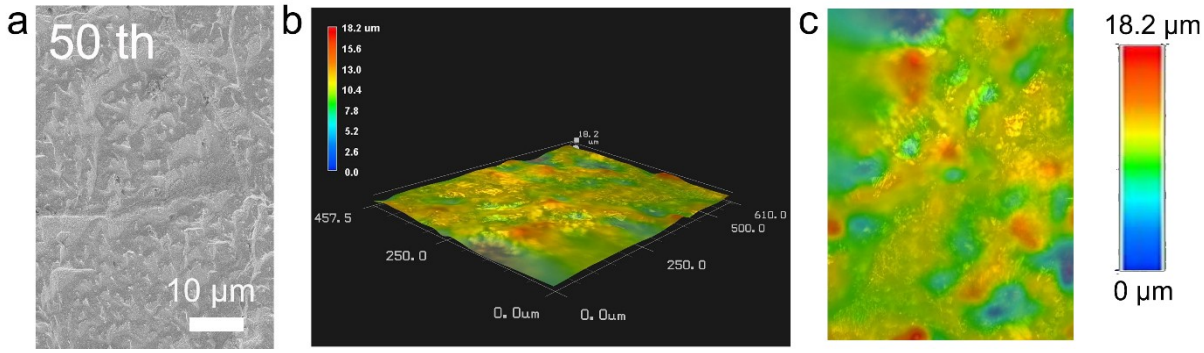

Figure S10. a) SEM image of Sn electrode after 50th cycle in alkaline electrolyte. The corresponding optical surface profilometry image of b) 3D and c) 2D features.

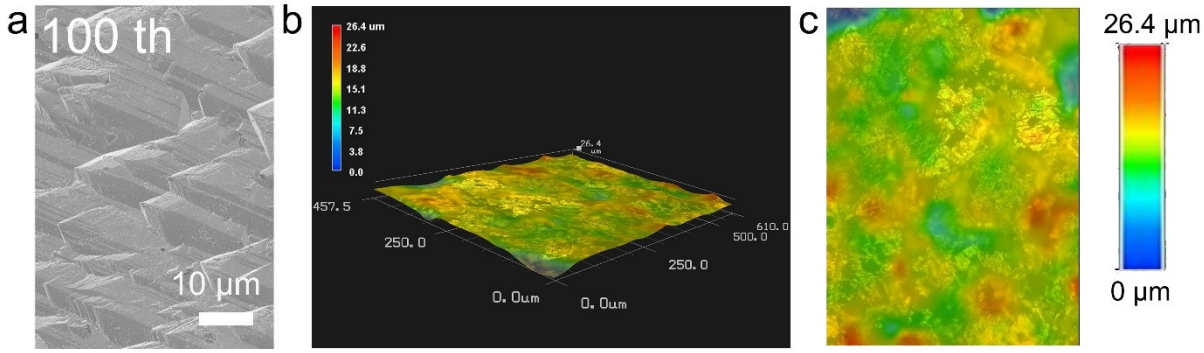

Figure S11. a) SEM image of Sn electrode after 100th cycle in alkaline electrolyte. The corresponding optical surface profilometry image of b) 3D and c) 2D features.

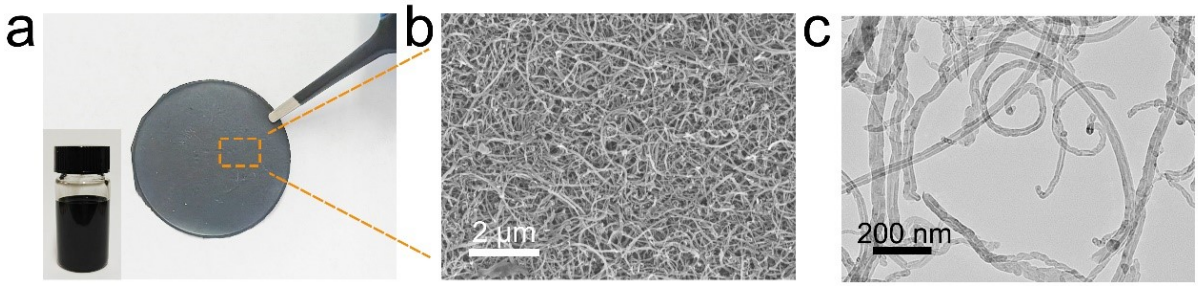

Figure S12. a) Optical photograph of the aqueous dispersion and self-assembly film of CNTs. The corresponding b) SEM and c) TEM images of the employed CNTs.

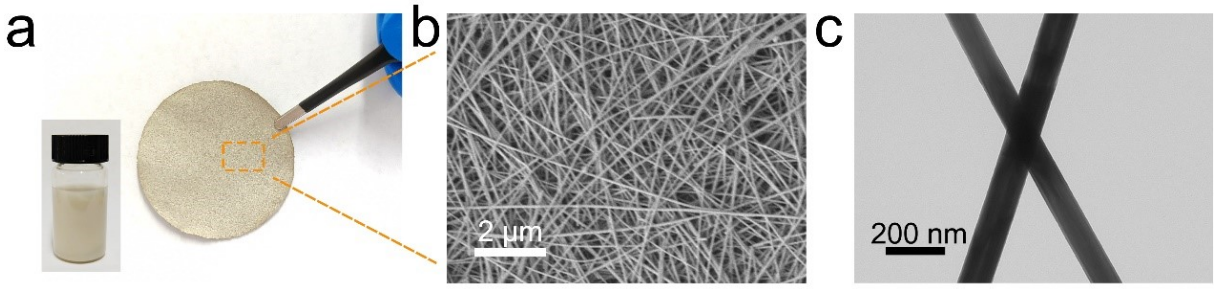

Figure S13. a) Optical photograph of the aqueous dispersion and self-assembly film of AgNWs. The corresponding b) SEM and c) TEM images of the employed AgNWs.

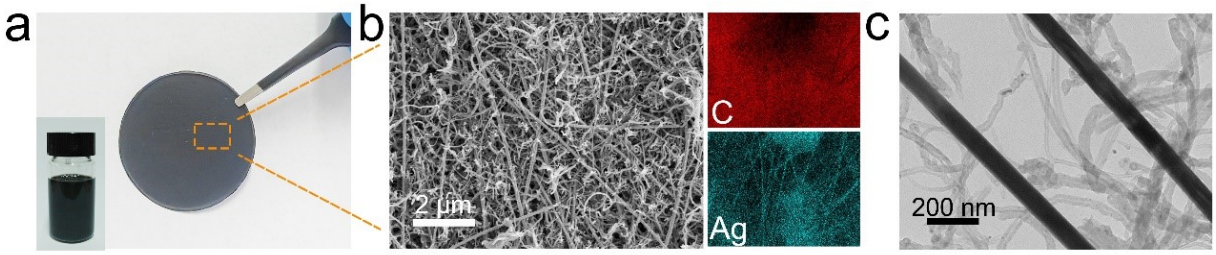

Figure S14. a) Optical photograph of the aqueous dispersion and hybrid film of AgNWs/CNTs cathode. b) The corresponding SEM image and element mapping for C and Ag, respectively; c) TEM image of the AgNWs/CNTs.

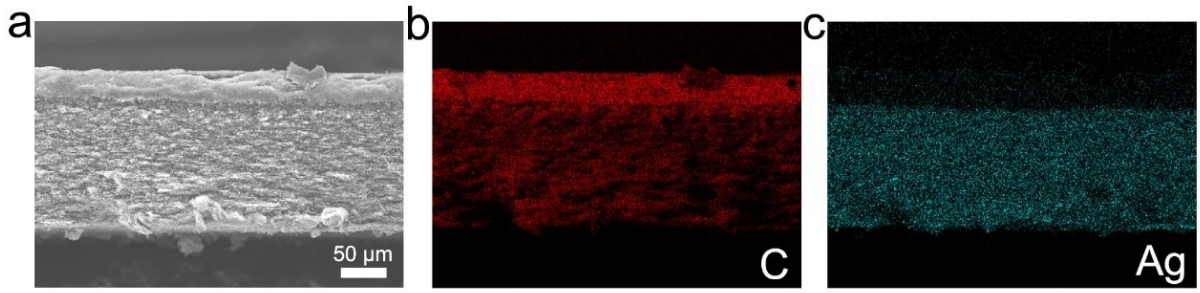

Figure S15. a) The cross-sectional SEM image of AgNWs/CNTs hybrid film. The corresponding element mapping for b) C and c) Ag element, respectively.

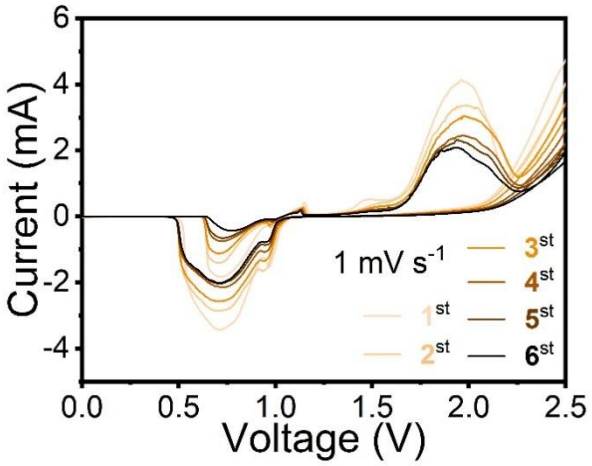

Figure S16. CV curves at 1 mV s^{-1} for the Sn-Ag cell without a cation-exchange membrane (CEM).

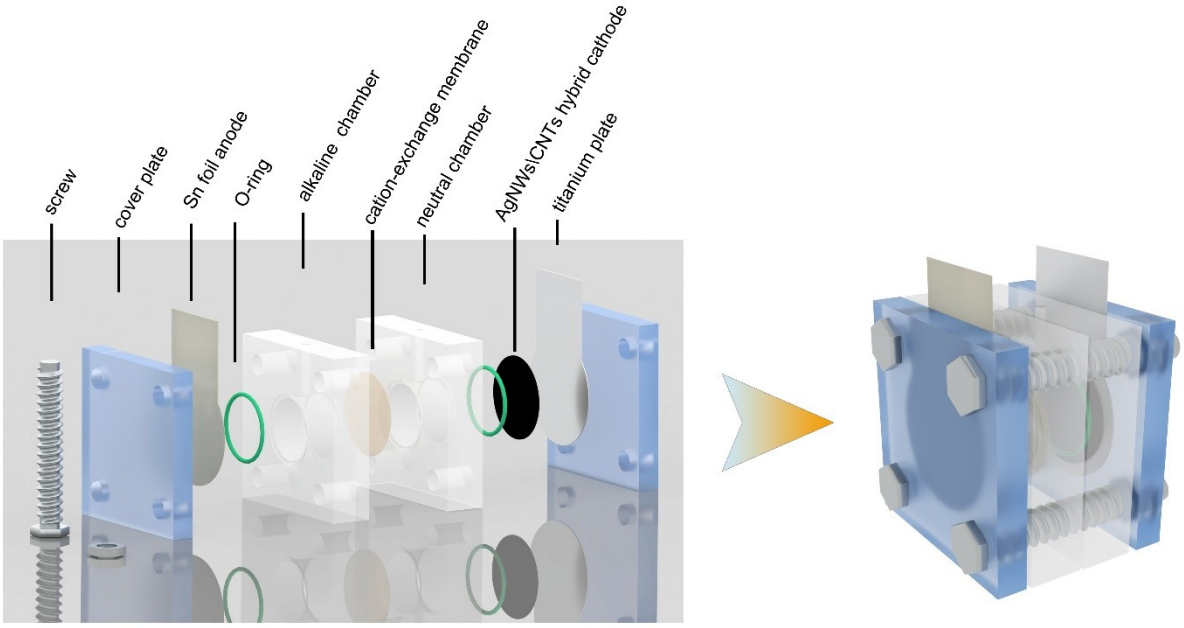

Figure S17. Schematic diagram of the decoupled Sn–Ag cell structure.

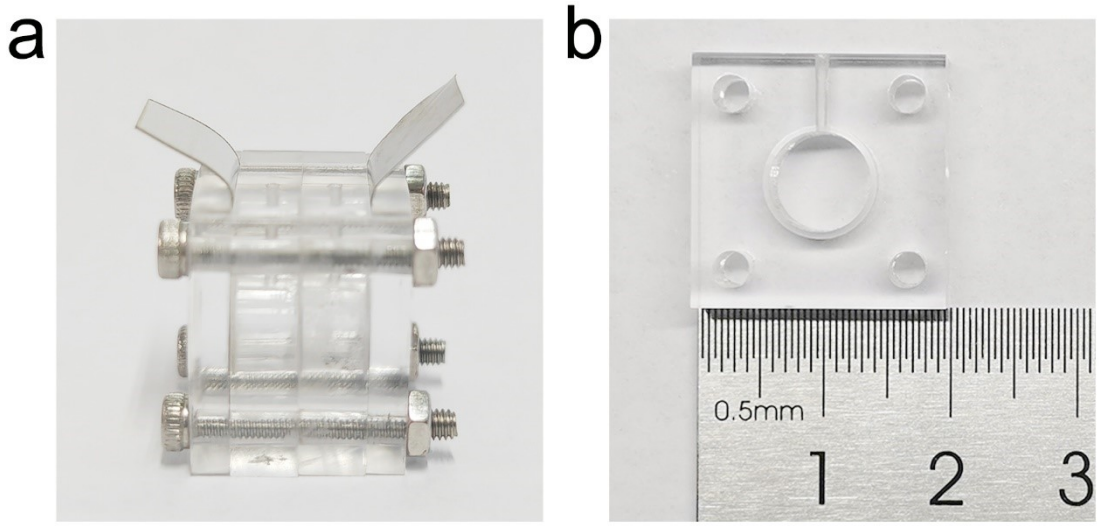

Figure S18. a) Optical photograph of the decoupled cell. b) The size of the chamber.

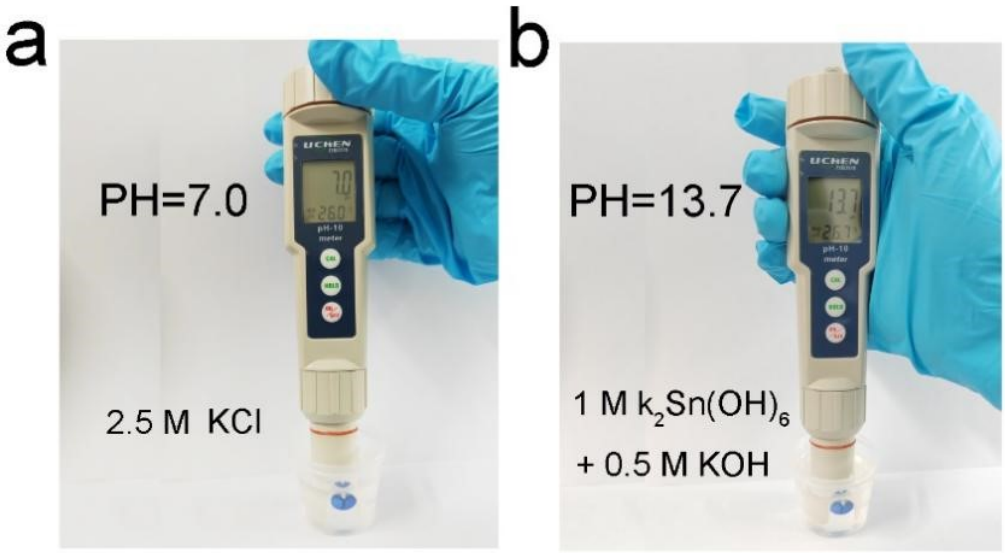

Figure S19. The initial pH value of electrolytes in a) cathode chamber and b) anode chamber.

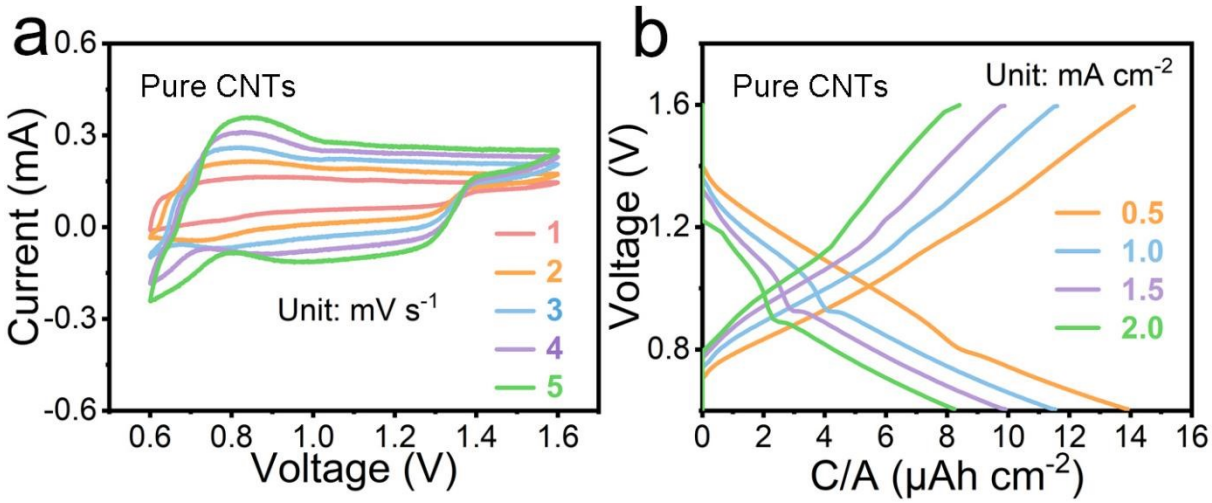

Figure S20. a) CV curves at varying scan rates, b) GCD curves at diverse current densities of the decoupled Sn-CNTs cell with pure CNTs electrode.

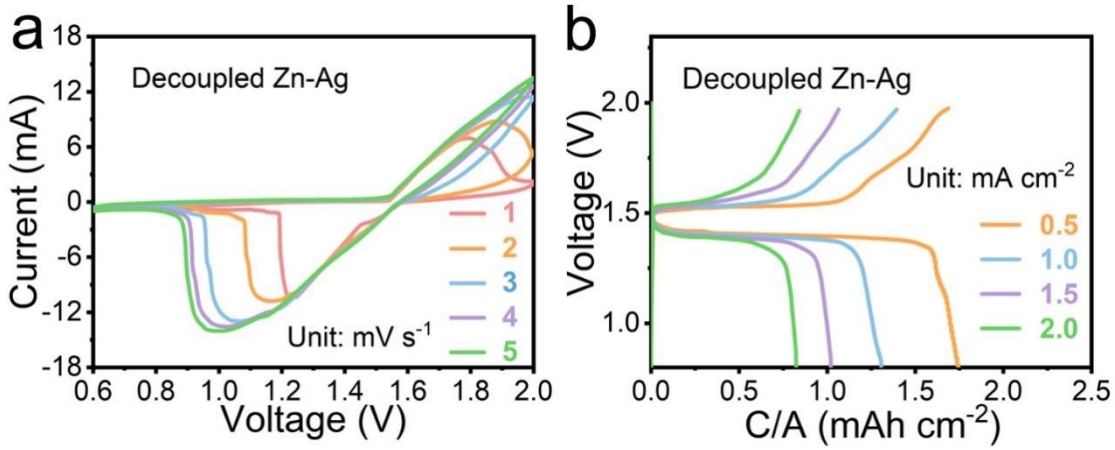

Figure S21. a) CV curves at varying scan rates, b) GCD curves at different current densities of the decoupled Zn-Ag cell.

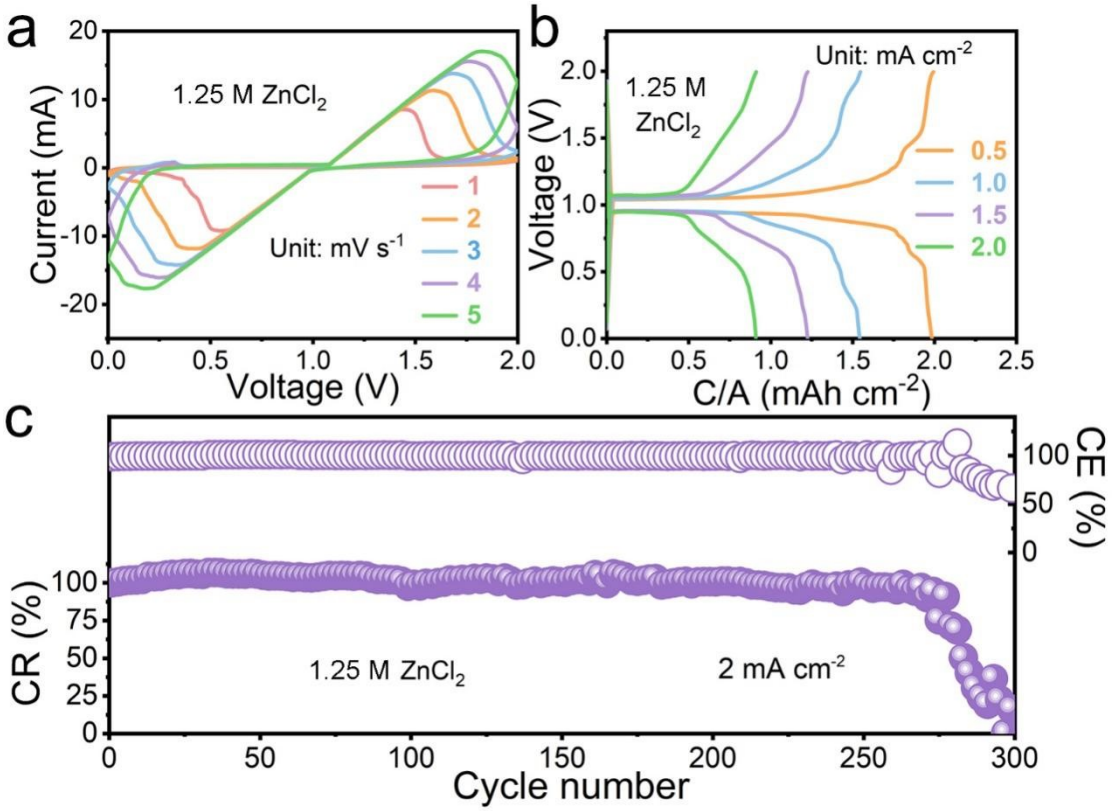

Figure S22. a) CV curves at varying scan rates, b) GCD curves at different current densities, and c) cyclic stability of the Ag-Zn full cell in 1.25 M $ZnCl_2$ without a CEM.

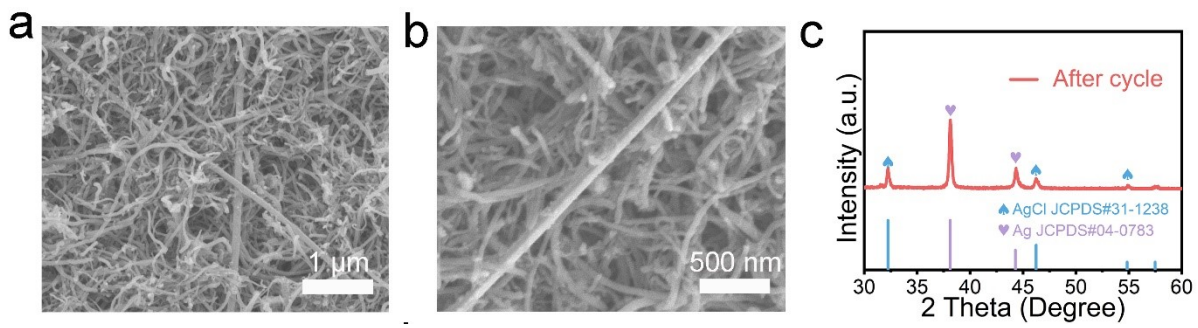

Figure S23. a, b) The SEM image and c) XRD pattern of AgNWs/CNTs hybrid cathode after cycle.

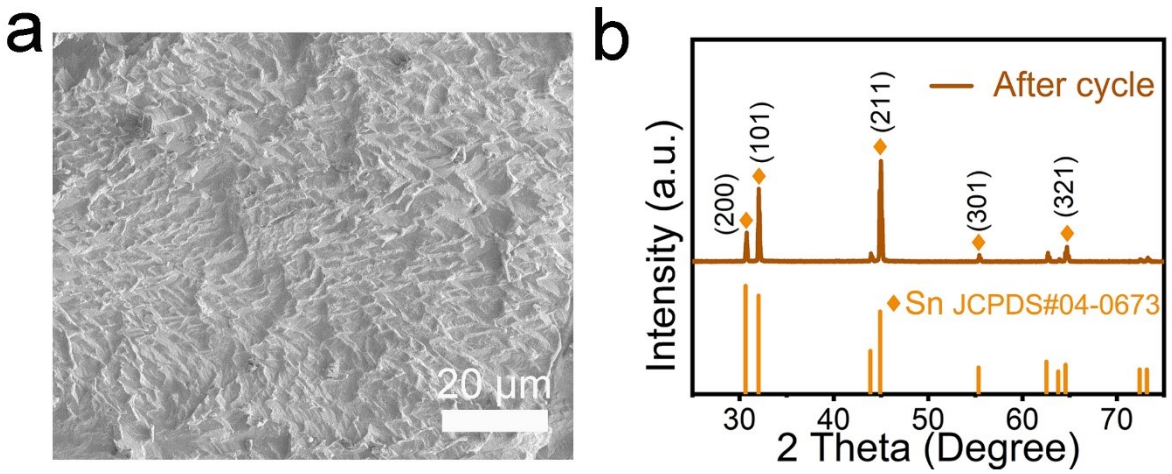

Figure S24. a) The SEM image and b) XRD pattern of Sn anode after cycle.

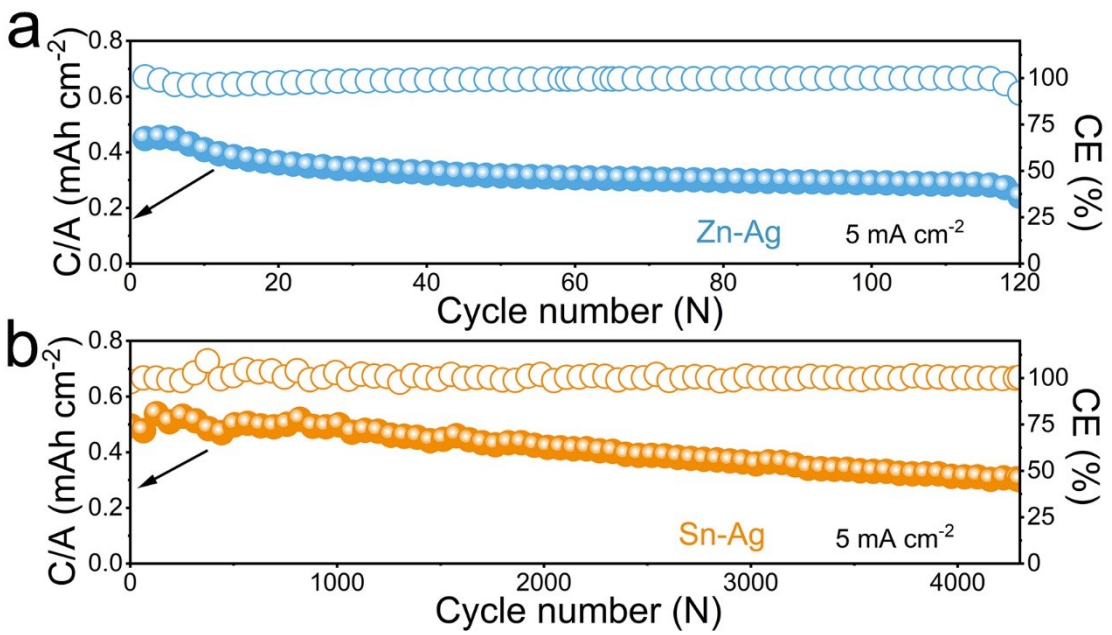

Figure S25. The cyclic stability at 5 mA/cm^2 of a) the decoupled Sn–Ag cell and b) the comparative decoupled Zn-Ag cell.

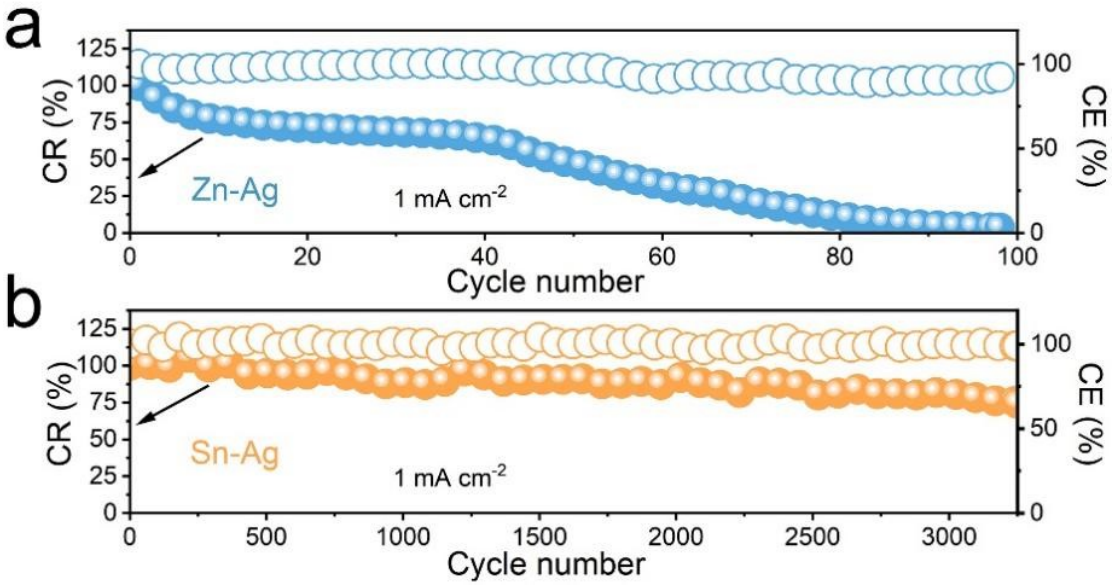

Figure S26. The cyclic stability at 1 mA/cm^2 of a) the decoupled Sn–Ag cell and b) the comparative decoupled Zn-Ag cell.

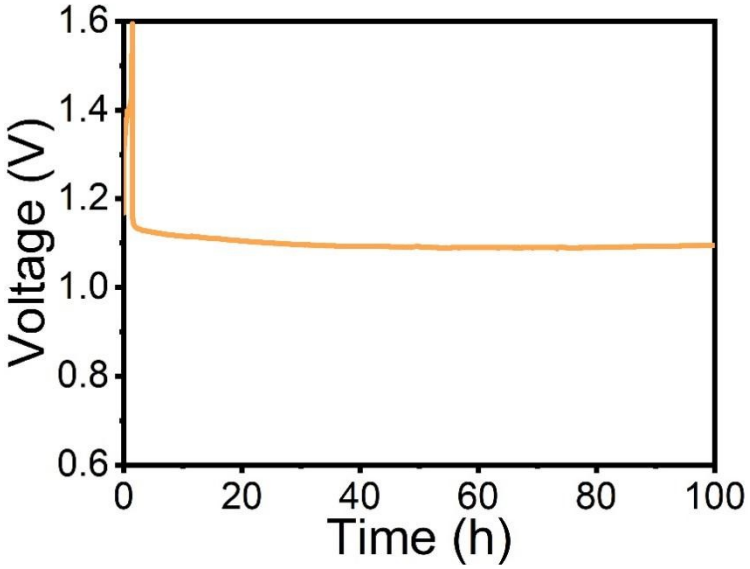

Figure S27. Self-discharge test of the decoupled Sn–Ag cell.

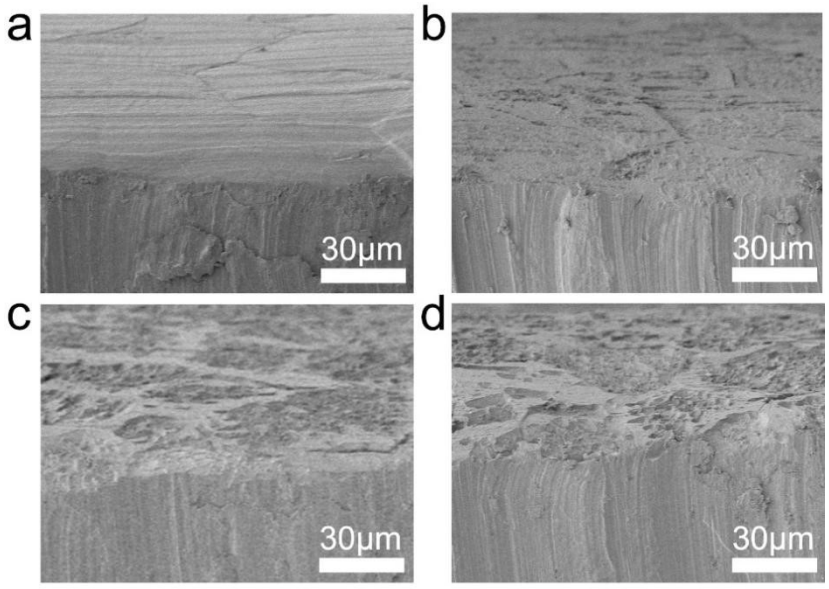

Figure S28. a) The cross-sectional SEM images of Sn during the charge-discharge process at the point of a) 1, b) 5, c) 6 and d) 7.

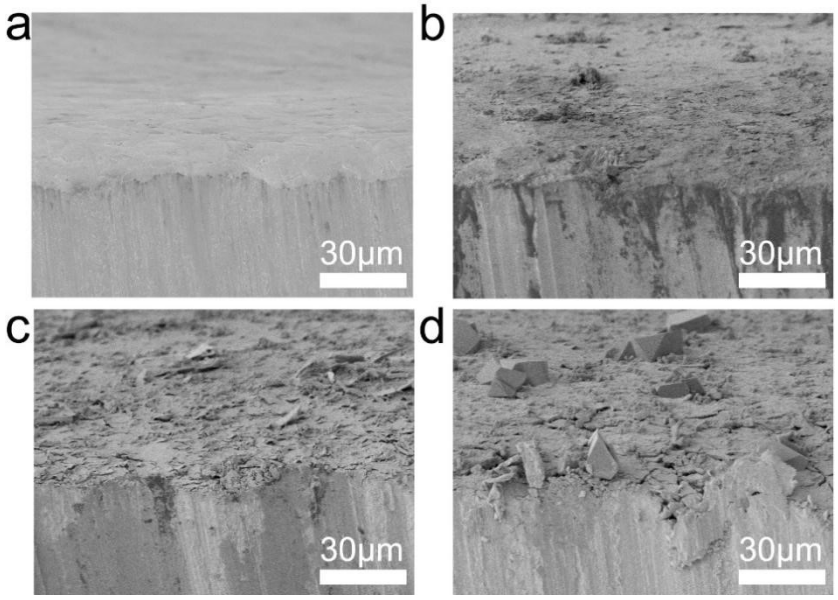

Figure S29. The cross-sectional SEM images of Zn during the charge-discharge process at points of a) 1, b) 5, c) 6 and d) 7.

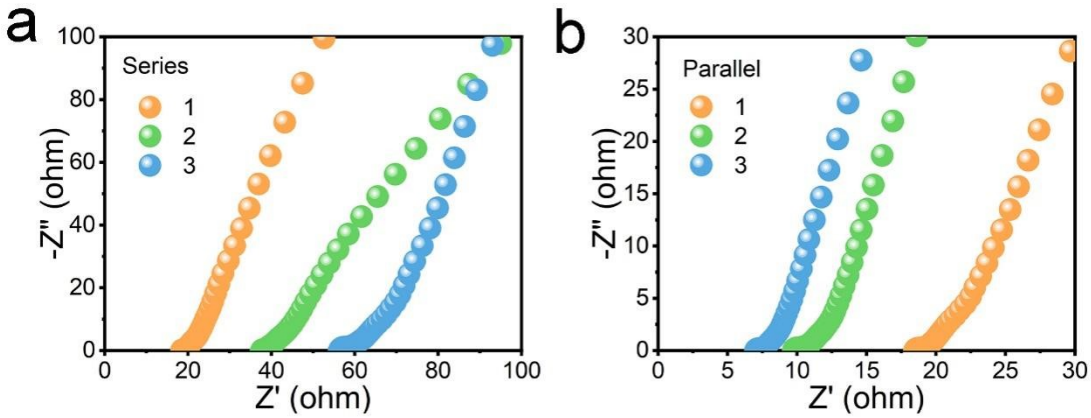

Figure S30. a) Comparison of EIS for single cell, two cells in series and three cells in series. b) Comparison of EIS for single cell, two cells in parallel and three cells in parallel.

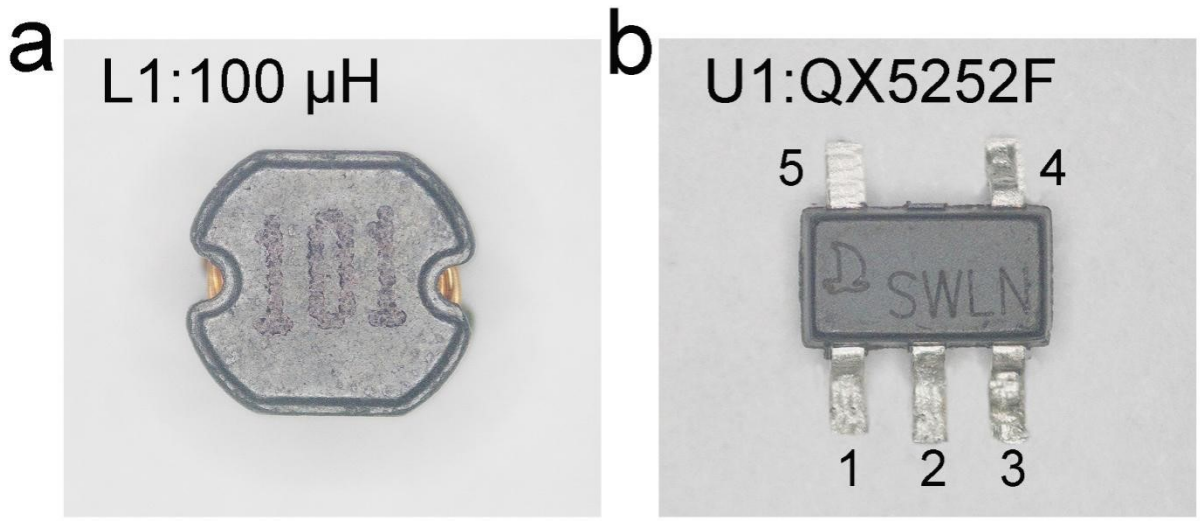

Figure S31. a) Inductors used in the application circuit of the intelligent power system. b) The component in the application circuit that controls circuit switching between day and night.

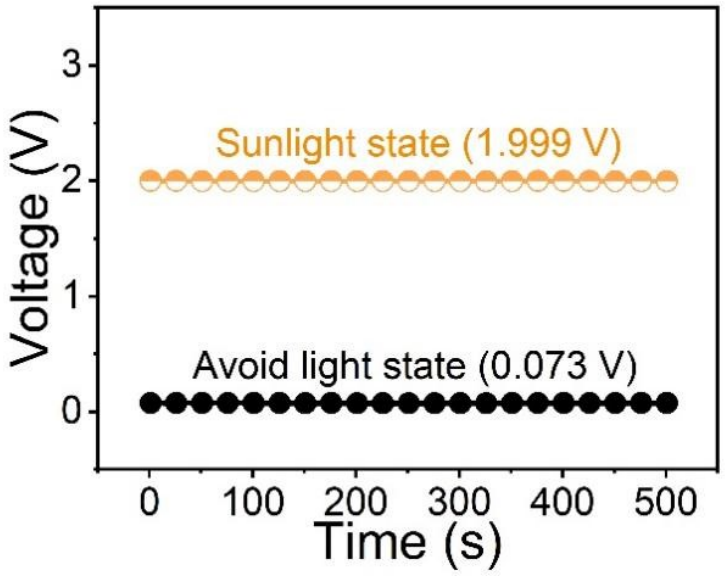

Figure S32. The output voltage of the integrated solar cell under different illumination conditions.